Joule

Article

Modular Electrochemical Synthesis Using a Redox Reservoir Paired with Independent Half-Reactions

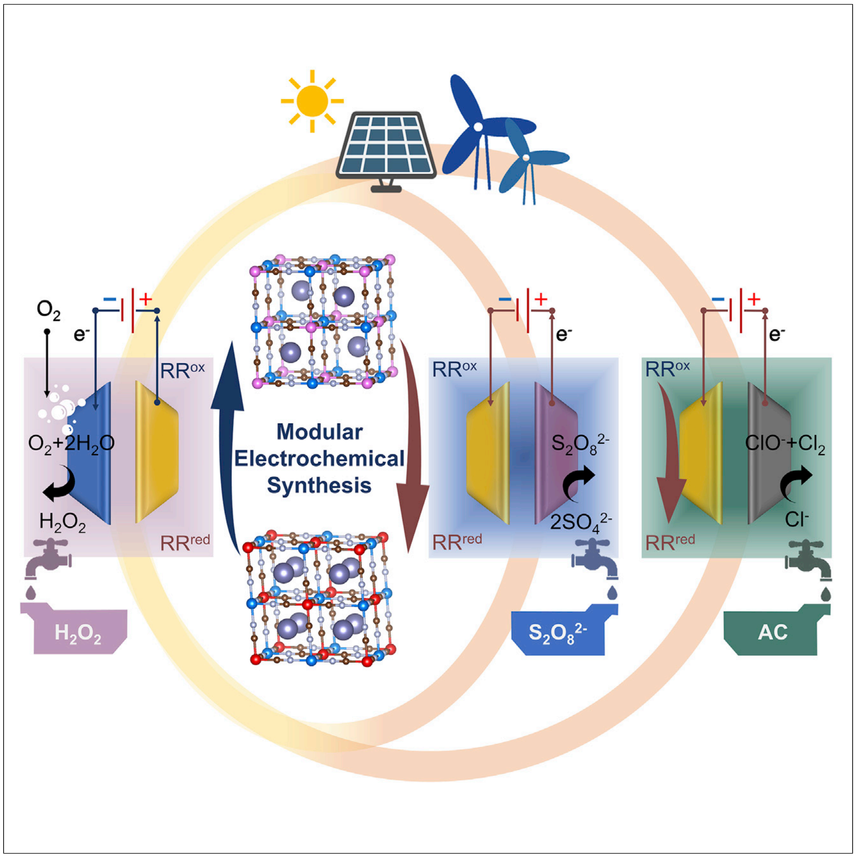

Solid-state redox-reservoir-enabled modular electrochemical synthesis (ModES) systems are shown to lift the constrains due to tightly coupled anodic and cathodic reactions in conventional electrochemical synthesis. The reversible oxidation/reduction of a sodium nickel hexacyanoferrate redox-reservoir electrode is paired with the reductive/oxidative half-reactions for producing hydrogen peroxide, sodium persulfate, or active chlorine in a modular and cyclic fashion on demand. This ModES system can be continuously operated with an excellent stability and high voltage efficiency.

Fengmei Wang, Wenjie Li, Rui Wang, ..., Hui-Chun Fu, Shannon S. Stahl, Song Jin

jin@chem.wisc.edu

HIGHLIGHTS

A new strategy for modular electrochemical synthesis (ModES) of valuable chemicals

Different oxidative and reductive half-reactions are paired in flexible ModES systems

A ModES system demonstrated with a heterogeneous NaNiHCF redox reservoir

Three strong oxidants, H_2O_2, $Na_2S_2O_8$, and active chlorine were produced on demand

Wang et al., Joule 5, 1–17
January 20, 2021 © 2020 Elsevier Inc.
https://doi.org/10.1016/j.joule.2020.11.011

Please cite this article in press as: Wang et al., Modular Electrochemical Synthesis Using a Redox Reservoir Paired with Independent Half-Reactions, Joule (2020), https://doi.org/10.1016/j.joule.2020.11.011

Joule

CellPress

Article

Modular Electrochemical Synthesis Using a Redox Reservoir Paired with Independent Half-Reactions

Fengmei Wang,[1,2] Wenjie Li,[1] Rui Wang,[1] Tianqi Guo,[1] Hongyuan Sheng,[1] Hui-Chun Fu,[1] Shannon S. Stahl,[1] and Song Jin[1,3,*]

SUMMARY

Electrochemical synthesis of high-value chemicals using renewable electricity could lead to sustainability advantages over conventional chemical manufacturing. The tight coupling between paired anodic and cathodic reactions in conventional electrochemical processes, however, constrains the products and their efficiencies. Here, we demonstrate a strategy to achieve modular electrochemical synthesis (ModES) of different chemicals by decoupling and pairing the oxidative and reductive half-reactions with a heterogeneous redox reservoir (RR). Specifically, sodium nickel hexacyanoferrate (Na-NiHCF) can serve as a robust and reversible RR that enables the modular production of several strong oxidants, hydrogen peroxide (H_2O_2) and sodium persulfate ($Na_2S_2O_8$) or active chlorine, in separate RR-coupled electrochemical processes. The system's excellent performance and operational stability is demonstrated by continuous operation over 100 cycles (~36 h) to produce H_2O_2 and $Na_2S_2O_8$ with a high voltage efficiency. The concept presented here highlights the prospects for using RRs to enable efficient, modular, and on-demand electrochemical synthesis of valuable chemicals.

INTRODUCTION

Electrochemical synthesis driven by electricity from renewable sources, such as wind, solar, and hydro power, rather than fossil fuels, offers a powerful and sustainable alternative to conventional chemical manufacturing for the production of inorganic or organic chemicals.[1–5] Electrochemical manufacturing is especially well suited for distributed production of low-to-medium volume high-value chemicals, rather than commodity chemicals that benefit from the economies of scale associated with current chemical processes.[6,7] Conventional electrochemical processes generate desired chemicals at the working electrode and are commonly coupled with a sacrificial half-reaction at the auxiliary electrode. For example, in solar fuel production, water oxidation is the sacrificial reaction that provides electrons and protons for hydrogen production or CO_2 reduction.[8–10] Smaller scale processes have more flexibility in the sacrificial half-reaction, although it is typically selected to minimize cost and the environmental footprint. For example, electrochemical oxidation reactions are often coupled to the reduction of protons or protic solvents to generate hydrogen gas, which may be collected and used for other applications or simply vented as a by-product. The inherent inefficiency associated with these sacrificial half-reactions has motivated the development of "paired electrolysis" methods that generate valuable products at both the anode and the cathode.[11,12] Paired electrolysis methods have been industrially deployed on large and small

Context & Scale

The electrochemical production of chemicals using renewable electricity has sustainability advantages over conventional chemical manufacturing, particularly for distributed on-site production of high-valued chemicals in small scale. However, anodic and cathodic reactions in conventional electrochemical synthesis are tightly coupled. The sacrificial reactions at the auxiliary electrodes often produce less valuable by-products, resulting in inefficiency and waste.

Here, a modular electrochemical synthesis strategy is developed so that various useful anodic and cathodic electrochemical half-reactions can be paired to increase efficiency and reduce product waste. Specifically, sodium nickel hexacyanoferrate redox reservoir was designed and paired with the production of three strong oxidants (hydrogen peroxide, sodium persulfate, and active chlorine) in different cells. This strategy enables an efficient on-demand electrochemical production of valuable chemicals using renewable electricity.

Please cite this article in press as: Wang et al., Modular Electrochemical Synthesis Using a Redox Reservoir Paired with Independent Half-Reactions, Joule (2020), https://doi.org/10.1016/j.joule.2020.11.011

scales, ranging from the chlor-alkali process for the production of chlorine and sodium hydroxide (tens of million tons per year[4]) to the parallel oxidation of 4-t-butyl-toluene to the aryl dimethyl acetal and reduction of dimethyl-*o*-phthalate to phthalide operated by BASF (several thousand tons per year[5,13]).

The development of paired electrolysis methods faces unique challenges and is not always successful. The simultaneous production of two products with fixed stoichiometry can present economic challenges associated with variable market demands for two different products.[14] The tight coupling between anodic and cathodic reactions could present conflicts for the two desired electrochemical half-reactions that may require different reaction conditions (e.g., the optimal solution pH and the solvents) or reaction rates. Furthermore, during conventional electrolysis, the reductive or oxidative production of different chemicals takes place simultaneously, such that the expensive ion-selective membranes must be used to separate the electrode processes to manage (selective) ion migration and avoid product crossover for high product purity.[15–17] It would be very attractive to be able to mix and match useful anodic and cathodic electrochemical half-reactions to access the benefits of paired electrolysis, while overcoming many of the challenges associated with their development, in order to maximize the efficiency and minimize the product waste and energy consumption of electrochemical manufacturing.

Here, we propose to develop new and general modular electrochemical synthesis (ModES) approaches without the use of membranes by using solid-state redox reservoirs (RRs), which consist of charge-carrying redox-active materials that can reversibly store and release electrons and ions (e.g., Na^+, H^+, and OH^-), to enable complete electrochemical reactions using independent half-reactions of our choice. The key to ModES is the use of redox reservoirs. Analogous to the water reservoirs used in the pumped hydroelectric storage, redox reservoirs allow temporary storage of the electrons and the chemical ions to redirect them for carrying out different electrochemical half-reactions, potentially at different times, locations, and/or scales of the reactions. Recent reports have demonstrated the production of hydrogen and oxygen gases via water splitting without product crossover by using redox mediators,[15,16,18–23] but such concepts have potential for even broader impact in modular on-demand electrochemical synthesis of valued-added chemicals[4–6,9,12] by pairing independent half-reactions. The flexible nature of ModES can eliminate constraints in conventional electrolysis approaches and enable previously unpaired electrochemical processes to be strategically paired.

To demonstrate the ModES concept, we specifically target the electrochemical production of two strong oxidants, hydrogen peroxide (H_2O_2) and sodium persulfate ($Na_2S_2O_8$). Both are widely used in chemical synthesis, electronics, disinfection, and water remediation and treatment,[7,24–26] with a considerable annual production scale and high value (about 5.5 × 10^6 tons for H_2O_2 with the total value of $4.4 billion in 2019,[27] and about 2 × 10^5 tons for $Na_2S_2O_8$ with a price of $1,600/ton[7,28]). There are significant cost and safety concerns in transporting and storing these strong oxidants in high concentration; yet, many applications, such as disinfection and environmental remediation, require very dilute concentrations. Therefore, distributed on-site production of H_2O_2 and $Na_2S_2O_8$ are especially desirable.[29] In conventional electrolysis approaches, hydrogen peroxide production reaction (HPR) via oxygen reduction [$O_2 + 2\,H_2O + 2\,e^- \rightarrow H_2O_2 + 2\,OH^-$, $E^\circ = 0.267$ V at pH = 7 versus standard hydrogen electrode (SHE)] is coupled to the oxygen evolution reaction (OER) (Figure 1A),[30] while persulfate production via the oxidation of sulfate ions (PSR, $2\,SO_4^{2-} \rightarrow S_2O_8^{2-} + 2\,e^-$, $E^\circ = 2.01$ V versus SHE) at the anode is coupled to the

[1]Department of Chemistry, University of Wisconsin-Madison, 1101 University Avenue, Madison, WI 53706, USA

[2]CAS Center for Excellence in Nanoscience, CAS Key Laboratory of Nanosystem and Hierarchical Fabrication, National Center for Nanoscience and Technology, Beijing 100190, China

[3]Lead Contact

*Correspondence: jin@chem.wisc.edu

https://doi.org/10.1016/j.joule.2020.11.011

Please cite this article in press as: Wang et al., Modular Electrochemical Synthesis Using a Redox Reservoir Paired with Independent Half-Reactions, Joule (2020), https://doi.org/10.1016/j.joule.2020.11.011

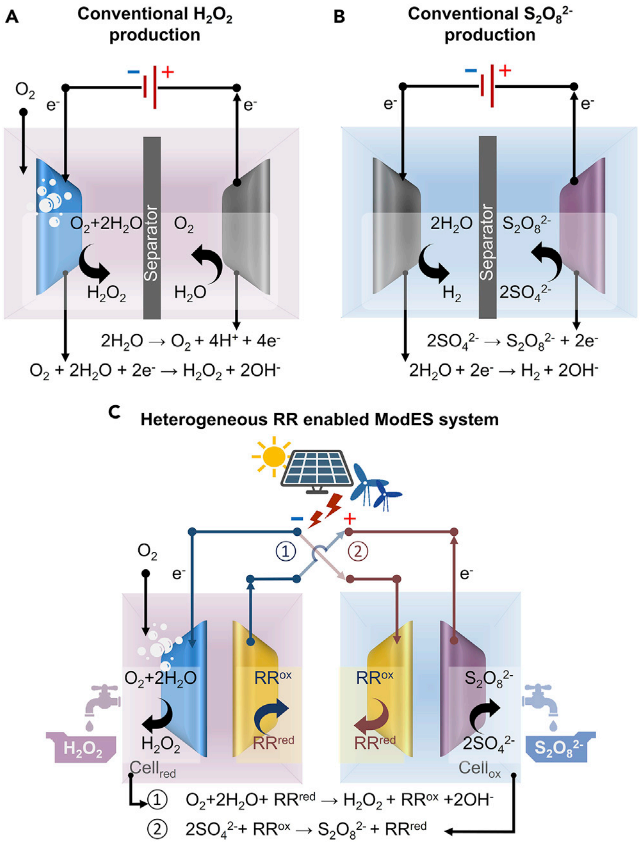

Figure 1. Schematic Illustration of the RR Enabled ModES System for Efficient Paired Synthesis of H_2O_2 and $Na_2S_2O_8$ in Comparison with Conventional Electrosynthesis Cells

(A) In a conventional electrosynthesis cell, HPR occurs on the cathode, along with OER on the anode at the same time. The anode and cathode compartments are separated by a membrane to prevent H_2O_2 crossover.

(B) In a conventional cell, PSR occurs on the anode, along with HER on the cathode separated by a membrane.

(C) In a ModES system, anodic and cathodic processes can be carried out independently to produce H_2O_2 and $S_2O_8^{2-}$ without a membrane in a modular fashion at the demanded rate and scale. This is enabled by the use of a redox reservoir (RR) that can store and release electrons/ions to pair up sequentially with the HPR and PSR reactions in two separate cells, denoted as the anodic (blue) and cathodic (red) cells, respectively. This ModES system can be continuously run to produce H_2O_2 and $S_2O_8^{2-}$ in different containers in a batch-wise fashion.

hydrogen evolution reaction (HER) at the cathode (Figure 1B).[31] These conventional processes produce H_2 and O_2 by-products at the counter electrodes, which are much less valuable than the strong oxidants themselves. Here, we design and demonstrate a ModES system enabled by a heterogeneous redox reservoir to produce H_2O_2 and $Na_2S_2O_8$ without sacrificial reagents or undesired by-products. We have identified a robust and reversible solid-state RR material, sodium nickel hexacyanoferrate (NaNiHCF), and optimized the electrocatalytic processes for HPR and PSR to enable a proof-of-concept ModES process that can be continuously operated over 100 cycles (~36 h) to produce useful concentrations of H_2O_2 and $Na_2S_2O_8$ in neutral solution with a high voltage efficiency.

Design of the Modular Electrochemical Synthesis System

To lift the constrains that the anodic and cathodic reactions must be performed simultaneously at the same scale, a ModES process is designed to realize modular

Please cite this article in press as: Wang et al., Modular Electrochemical Synthesis Using a Redox Reservoir Paired with Independent Half-Reactions, Joule (2020), https://doi.org/10.1016/j.joule.2020.11.011

synthesis of two chemicals without a membrane. As illustrated in Figure 1C, it consists of two electrochemical cells to separately and sequentially produce H_2O_2 and $Na_2S_2O_8$, each paired with a common RR electrode. When H_2O_2 solution is needed, HPR is conducted on the cathode coupled with the oxidation of the RR electrode to oxidized state (RR^{ox}) in the left cell ($Cell_{red}$); when $Na_2S_2O_8$ solution is needed, PSR is conducted on the anode coupled with the reduction of the RR electrode to reduced state (RR^{red}) in the right cell ($Cell_{ox}$). The heterogeneous RR electrode is reversibly oxidized and reduced between RR^{red} and RR^{ox} to store and release electrons and ions. With the use of RR, in principle, the anodic and cathodic processes do not need to be matched in terms of production time and scale, and thus, can be carried out on demand by mechanically swapping the heterogeneous RR electrodes between the two cells for producing H_2O_2 and $S_2O_8{}^{2-}$ in a modular and cyclic fashion.

RESULTS AND DISCUSSION

Synthesis and Electrochemical Properties of NaNiHCF as a Solid-State Redox Reservoir

An ideal heterogeneous RR material should incorporate several features: proper redox potential, fast redox kinetics, robust stability, high charge-storage capacity, and low fabrication cost. Considering the redox potential of hydrogen peroxide production ($E^\circ = 0.267$ V versus SHE at pH = 7) and persulfate production ($E^\circ = 2.01$ V versus SHE) reactions that we target, the redox potential of RR material should be within 0.27–2.01 V (versus SHE). Our initial screening focused on the electrode materials that are commonly used in aqueous batteries (including Na^+, Li^+, etc.) with high capacity and good stability in neutral solutions.[32] Following these considerations, we chose Prussian blue analogs that are commonly used in the aqueous batteries as the RR material due to their open framework architecture, which provides highly reversible intercalation and de-intercalation of ions (Li^+, Na^+ etc.).[32–34] After some preliminary screening, we specifically targeted sodium nickel hexacyanoferrate (NaNiHCF) as the RR electrode material for producing H_2O_2 and $Na_2S_2O_8$ in the ModES system. The NaNiHCF samples with a rhombohedral phase were synthesized using a kinetically controlled co-precipitation reaction.[35] During the synthesis process, sodium citrate was added to form Ni^{2+}-citrate chelate, which slowly released the Ni^{2+} ions to react with $Fe(CN)_6{}^{4-}$ ions to precipitate NaNiHCF (see Experimental Procedures for details). By tuning the ratio between Ni^{2+} and sodium citrate (1: *x*), we could control the morphology and size of the NaNiHCF crystals (denoted as NaNiHCF-*x*), without changing their crystal phase (Figures S1 and S2). The scanning electron microscopy (SEM) image of the representative NaNiHCF-10 crystals (Figure 2A) showed well-faceted microcubes. The powder X-ray diffraction (PXRD) pattern collected on NaNiHCF-10 sample (Figure 2B) nicely fit the rhombohedral structure[36,37] with obvious doublet diffraction peaks at (220), (420), (440), and (620), in comparison with the standard pattern of the cubic phase (JCPDS no. 52-1907). The elemental analysis by inductively coupled plasma-optical emission spectroscopy (ICP-OES, Table S1) and energy dispersive X-Ray spectroscopy (EDS, Figures S1B–S1H) confirmed the compositions of Na, Ni, and Fe elements. Thermogravimetry analyses (TGA, Figure S3) revealed the water content in these NaNiHCF samples. The exact chemical composition of NaNiHCF-10 crystals was then found to be $Na_{2.36}Ni[Fe(CN)_6]_{1.09}\cdot 1.7\ H_2O$ with a near unity Ni/Fe ratio and enriched Na^+. The large amount of Na^+ ions in the crystal lattice led to the expansion of the unit cell and the reduction of crystal symmetry from cubic to rhombohedral.

The reversible redox reaction of NaNiHCF involves the transition of redox states between Fe^{III}/Fe^{II} and Na^+ ion insertion/extraction, along with a crystal structure phase transition between the rhombohedral and cubic phases (Figures 2C and S4).[38] The

Please cite this article in press as: Wang et al., Modular Electrochemical Synthesis Using a Redox Reservoir Paired with Independent Half-Reactions, Joule (2020), https://doi.org/10.1016/j.joule.2020.11.011

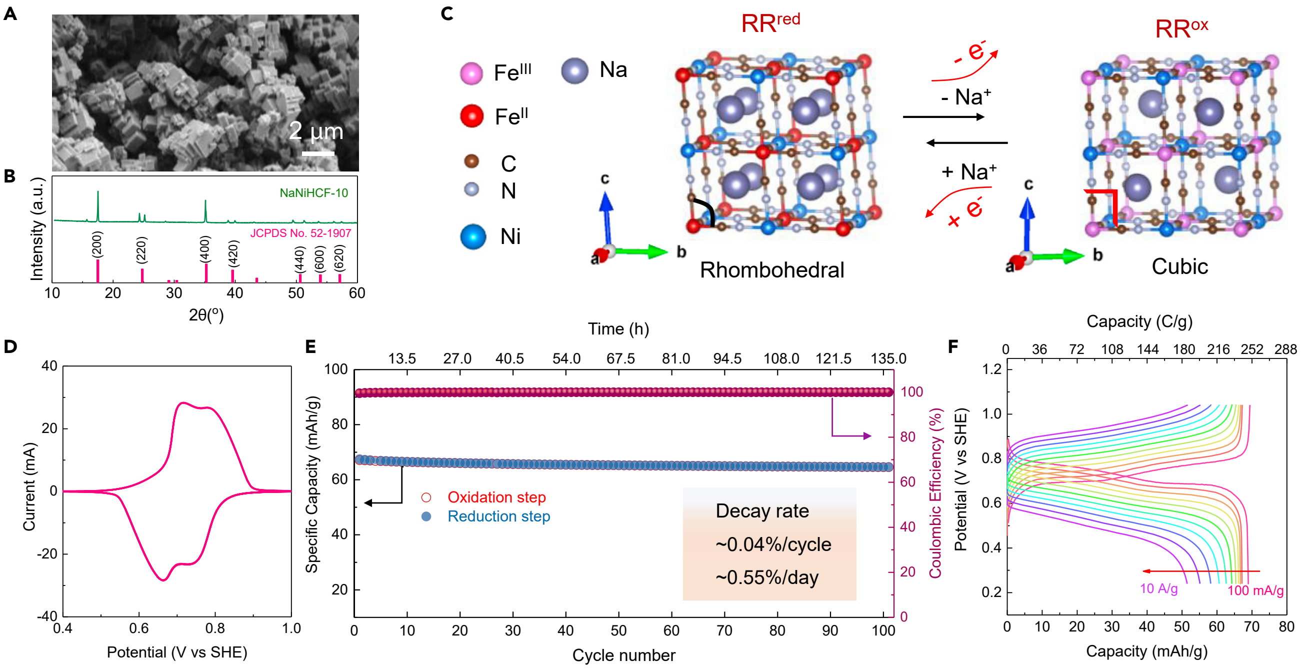

Figure 2. Structural and Electrochemical Characterizations of the NaNiHCF RR Material

(A and B) SEM image (A) and PXRD pattern (B) of the as-prepared NaNiHCF-10 crystals, which was synthesized with the molar ratio of 1: 10 between Ni^{2+} and sodium citrate during the co-precipitation synthesis.

(C) Illustration of the structure transition of the NaNiHCF material between the reduced (rhombohedral phase) and oxidized (cubic phase) states through reversible sodium ion insertion/extraction.

(D) Cyclic voltammetry of NaNiHCF-10 electrode scanned at 2 mV/s. The well resolved redox peaks correspond to the Fe^{III}/Fe^{II} redox couple with Na^+ insertion.

(E) Specific capacity and Coulombic efficiency (CE) of the electrode cycled at 100 mA g^{-1} for 100 cycles with cut-off potentials of 0.2 and 1.0 V_{SHE}.

(F) Representative galvanostatic redox curves of the electrode cycled at different rates of 0.1 A g^{-1} to 10 A g^{-1}. All electrochemical characterizations were performed in 1.7 M Na_2SO_4 electrolyte.

equilibrium potential of NaNiHCF electrode also changes with the state of the redox reservoir [SOR = $[Fe^{III}] / ([Fe^{III}] + [Fe^{II}]) \times 100\%$]. To carefully study the electrochemical behaviors of the NaNiHCF electrodes, cyclic voltammetry was performed at a scan rate of 2 mV s^{-1} between 0.24–1.1 V_{SHE} in 1.7 M Na_2SO_4 electrolyte (Figure 2D). The data revealed good electrochemical reversibility and a formal potential of 0.7 V_{SHE} for NaNiHCF, which falls in the window between the onset potentials for the H_2O_2 production (0.1 V_{SHE}) and $Na_2S_2O_8$ production (2.6 V_{SHE}) in neutral electrolyte (more discussion in the following section). After testing the whole series of NaNiHCF-x electrodes (Figure S5; Table S2), we found that the NaNiHCF-10 electrode has the best cycling stability. Galvanostatic cycling measurements of the NaNiHCF-10 electrode at a rate of 100 mA g^{-1} showed an initial capacity of 67.5 mAh g^{-1} (243 C g^{-1}), a low capacity decay rate of 0.04%/cycle (0.55%/ day), a high Coulombic efficiency (CE) of 99.9%, and an energy efficiency of 98% within 100 cycles (Figures 2E and S6). The cycling measurements also revealed the NaNiHCF-10 electrode could retain 77.6% of its capacity at a high rate of 10 A g^{-1}, indicating good electrochemical kinetics (Figures 2F and S7). Furthermore, the total electrode capacity could be easily scaled up without sacrificing the electrochemical performance by stacking multiple individual NaNiHCF-10 electrodes (1 × 1 cm^2 each) in parallel (Figure S8).

Investigation of HPR and PSR in Conventional Electrolysis

Considering that a neutral pH is ideal for on-site water remediation and many other environmental or disinfection applications,[26,30] the two reactions were investigated

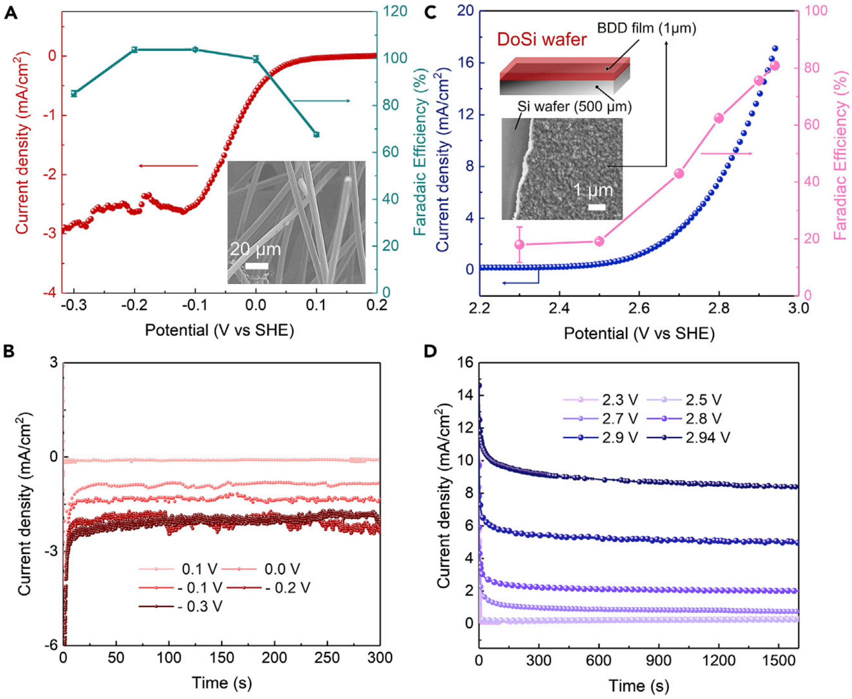

Figure 3. Investigation of Separate Electrochemical H_2O_2 and $Na_2S_2O_8$ Production in Conventional Divided Cells in a Neutral Electrolyte (1.7 M Na_2SO_4)

(A) LSV curve measured at a scan rate of 10 mV s^{-1} and the corresponding potential-dependent Faradaic efficiency of the treated carbon felt electrode for HPR. Inset shows the SEM image of the carbon felt electrode. The error bars shown are the confident intervals of the Faradaic efficiency at different potential.

(B) Chronoamperometry curves of the treated carbon felt electrode measured at various potentials.

(C) LSV curve measured at a scan rate of 10 mV s^{-1} and the corresponding potential-dependent Faradaic efficiency of the DoSi electrode for PSR. Insets show a schematic structure and a top-view SEM image of the DoSi wafer. The error bars shown are the confident intervals of the Faradaic efficiency at different potential.

(D) Chronoamperometry curves of the DoSi electrode for cumulative production of $Na_2S_2O_8$ measured at various potentials.

in a near neutral electrolyte 1.7 M Na_2SO_4 (pH = 6.2–6.5), which is also utilized in the electrochemical characterization of the NaNiHCF electrodes. For the H_2O_2 production, various carbon materials[26,39] have been developed to catalyze the HPR in alkaline and neutral solutions. We chose the commercial carbon felt knitted using carbon fibers with 10 μm diameter (see representative images in Figures 3A (inset) and S9) that has been widely used as electrode material for various electrochemical applications[40] due to its low cost and high surface area. To improve the hydrophilicity and activity of the carbon felt, it was heated at 400°C for 24 h in air to introduce surface functional groups, such as ethers (C–O–C) and carboxylic acids (O=C–OH).[26,39,41] High-resolution X-ray photoelectron spectroscopy (XPS) spectra de-convolved from C and O 1s signals confirmed that these functional groups were enriched after the heating treatment (Figure S10). We then used a divided H-cell with a Nafion 117 membrane to evaluate the electrocatalytic activity of the heat-treated carbon felt electrode in 1.7 M Na_2SO_4 electrolyte. The linear scan voltammetry (LSV) measurement of the carbon felt electrode showed an onset potential at an overpotential of 0.206 V (0.1 V_{SHE}, determined at a current density of 0.1 mA cm^{-2}), indicating good electrocatalytic activity (Figures 3A and S11). The high cumulative Faradaic efficiency of 100% (Figure 3A, green line) under the potential range of 0.0–0.2 V_{SHE}

Please cite this article in press as: Wang et al., Modular Electrochemical Synthesis Using a Redox Reservoir Paired with Independent Half-Reactions, Joule (2020), https://doi.org/10.1016/j.joule.2020.11.011

was determined by chronoamperometry (Figure 3B) and a subsequent product analysis by chemical titrations (Figure S12 and Section S1).[39,42] Note that the reduced Faradaic efficiencies observed below –0.3 V_{SHE} is caused by the mass transport limit of O_2 in electrolyte. These chronoamperometric tests at fixed applied potentials also confirmed the good stability of the carbon felt electrode for HPR.

In order to enable efficient PSR ($2\ SO_4^{2-} \rightarrow S_2O_8^{2-} + 2e^-$)[43,44] in neutral solution at high potential (>2.01 V_{SHE}), the competing reaction of oxygen evolution must be suppressed; thus, we specifically focused on electrodes with high overpotentials for OER. Boron-doped diamond (BDD) films are ideal for extreme oxidation electrochemistry due to their low catalytic activity for OER, chemical inertness, and a wide electrochemical stability window.[45,46] Therefore, a thin BDD film deposited on a heavily doped p type silicon wafer, denoted as DoSi (insets of Figures 3C and S13), was used to fabricate the working electrodes for PSR (see details in Experimental Procedures and Figure S14). The LSV curve of the DoSi electrode (Figure S15) measured in a divided cell using 1.7 M Na_2SO_4 electrolyte showed that the anodic current density increased rapidly when the applied potential increased above 2.6 V_{SHE} (Figure 3C, blue curve). Furthermore, the potential-dependent Faradaic efficiencies (Figure 3C, purple dots) of $Na_2S_2O_8$ production were obtained by chronoamperometric measurement under various potentials (Figure 3D), combined with iodometric detection (see details in Experimental Procedures and Figure S16). The Faradaic efficiency increased with the applied anodic potentials, with values of ~62% and ~76% at 2.8 V and 2.9 V_{SHE}, respectively. These measurements confirmed the good performance and stability of DoSi electrode for PSR in neutral solution.

Modular Production of H_2O_2 and $Na_2S_2O_8$ in a RR-Enabled ModES System

For the electrosynthesis demonstration, a two-cell ModES approach was used to produce H_2O_2 and $Na_2S_2O_8$. One NaNiHCF-10 electrode with an initial total capacity of 9.2 C (36.5 mg mass loading) was used as the RR electrode. In the first step, H_2O_2 was produced on the carbon felt electrode, while the reduced NaNiHCF-10 RR electrode (RR^{red}) was oxidized to RR^{ox} in the H_2O_2 cell ($Cell_{H_2O_2}$) (see Experimental Procedures and Figure S17). Specifically, the HPR on the carbon felt electrode was carried out under a constant potential of –0.1 V_{SHE}. After the H_2O_2 production step, the RR^{ox} electrode was transferred to $Cell_{S_2O_8^{2-}}$, in which, the PSR was carried out on the DoSi electrode at 2.74 V_{SHE} along with the regeneration of the RR^{ox} electrode back to its initial state (RR^{red}) to complete one ModES operation cycle. The Faradaic efficiencies of the HPR and PSR in the ModES system were calculated based on the amounts of the accumulated H_2O_2 and $Na_2S_2O_8$ in their respective cells (see Experimental Procedures for chemical quantitation details). Figure 4A shows the cumulative concentrations of the H_2O_2 and $Na_2S_2O_8$ products in 35 mL electrolyte solutions and the corresponding Faradaic efficiencies when the capacity utilization rate ($\frac{Utilized\ capacity\ of\ RR}{Total\ capacity\ of\ RR} \times 100\%$) of the RR electrode was controlled to different SORs within one ModES cycle. When the capacity of this specific RR electrode (9.2 C) was fully utilized, about 1.3 mM H_2O_2 and 0.7 mM $Na_2S_2O_8$ in 35 mL of electrolyte solutions could be produced.

To evaluate the reusability (or cyclability) of the ModES system for the modular production of H_2O_2 and $Na_2S_2O_8$, we carried out continuous consecutive production of these two chemicals by cycling the same RR electrode between 25% and 75% SOR (the corresponding capacity was around 4.6 C, see Experimental Procedures). As the electrochemical reactions proceeded, during the H_2O_2 production (or $Na_2S_2O_8$ production) step, the potential of RR electrode (E_{RR}, Figure S18A) and the cell voltage (V_{cell}, Figure S18B) in $Cell_{H_2O_2}$ (or $Cell_{S_2O_8^{2-}}$) increased (or decreased) with a consistent

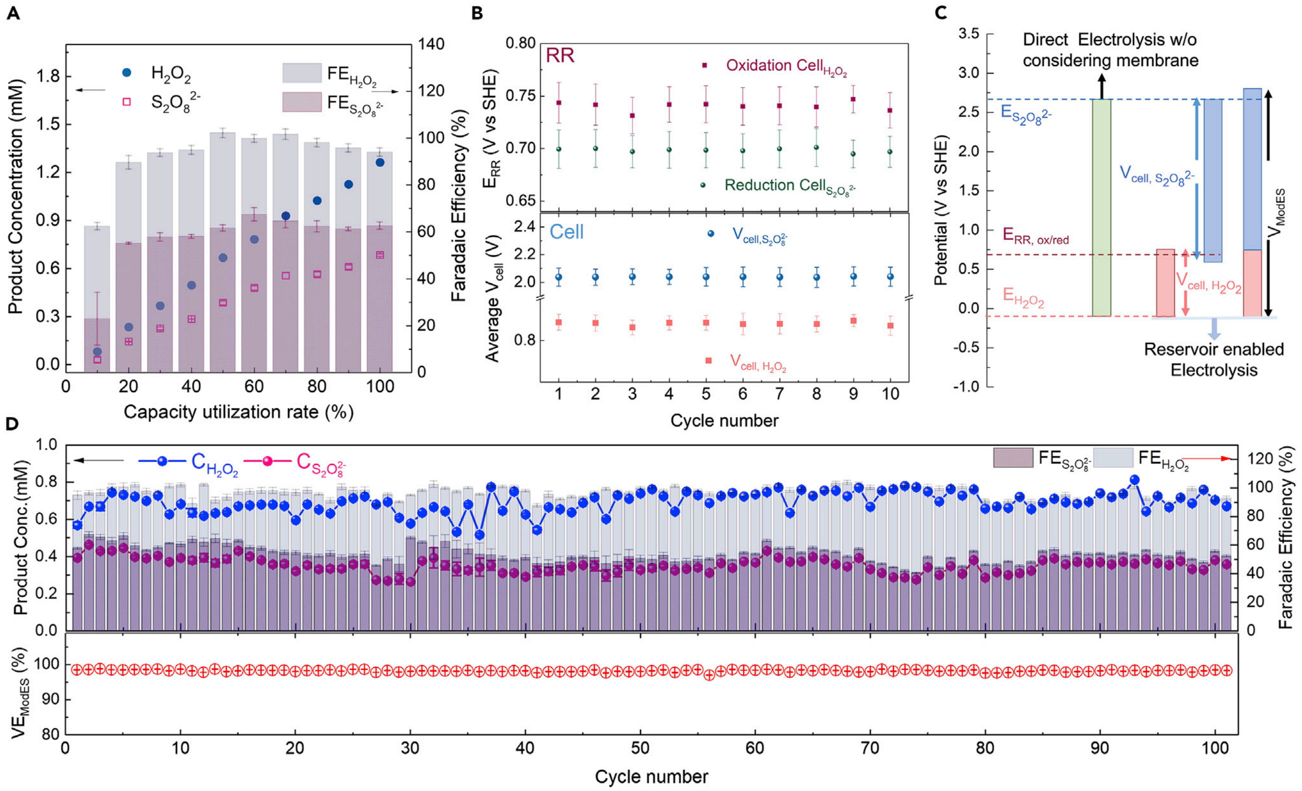

Figure 4. Modular Electrosynthesis of H_2O_2 and $Na_2S_2O_8$ in a Heterogenous RR-Enabled ModES System

(A) The accumulated concentrations of H_2O_2 (at −0.10 V_{SHE}) and $Na_2S_2O_8$ (at 2.74 V_{SHE}) products in 35 mL 1.7 M Na_2SO_4 electrolyte solutions and the corresponding Faradaic efficiencies at different capacity utilization rate of the NaNiHCF-10 RR electrode (2 × 2 cm^2, ~36.5 mg mass loading) within one ModES cycle. The error bars shown are the confident intervals of the product concentration and Faradaic efficiency.

(B) The average and the range of the potentials for the RR electrode (E_{RR}, top panel) and the corresponding average cell voltages (V_{cell}, bottom panel) of $Cell_{H_2O_2}$ and $Cell_{S_2O_8^{2-}}$ in ten representative cycles by cycling the RR electrode between 25% and 75% SOR. The error bars shown are the range of the potential profiles of the RR electrode and the whole cell.

(C) Alignments of electrochemical potentials and the comparison of cell voltages involved in this RR-enabled ModES system. The operating potentials for HPR and PSR are denoted as $E_{H_2O_2}$ and $E_{S_2O_8^{2-}}$, respectively. The total voltage applied to the ModES system is V_{ModES}. The voltage efficiency (VE) could be obtained through the following equation: $VE(\%) = (E_{S_2O_8^{2-}} - E_{H_2O_2}) / V_{ModES} \times 100\%$.

(D) Modular production of H_2O_2 and $Na_2S_2O_8$, showing the concentrations of ~0.7 mM (blue dots) and ~0.4 mM (purple dots), along with the Faradaic efficiencies (bars) achieved in each operation cycle, over 100 continuous cycles using this ModES system by cycling between 25% and 75% SOR of the RR electrode. The bottom panel shows the corresponding VE of this ModES system. The error bars shown are the confident intervals of the product concentration and Faradaic efficiency during the continuous operation.

pattern, as expected. The E_{RR} in $Cell_{H_2O_2}$ increased from 0.72 to 0.78 V_{SHE} with an average value of 0.75 V_{SHE} integrated over the whole cycle (Figure 4B, top panel, purple), which then decreased in $Cell_{S_2O_8^{2-}}$ from 0.72 to 0.68 V_{SHE} with an average value of 0.70 V_{SHE} (Figure 4B, top panel, green). Correspondingly, the overall cell voltage changed from 0.82 to 0.88 V ($Cell_{H_2O_2}$) and 2.02 to 2.06 V ($Cell_{S_2O_8^{2-}}$) with an average value of 0.85 V and 2.04 V (Figure 4B, bottom panel), respectively. To quantitatively evaluate the overall efficiency of the ModES system, we defined a voltage efficiency (VE) for this system. As illustrated in Figure 4C,

$$VE(\%) = V_{DIR} \Big/ V_{ModES} \times 100\% = \left(E_{S_2O_8^{2-}} - E_{H_2O_2}\right) \Big/ V_{ModES} \times 100\%$$

where, V_{DIR} is the operating potential difference between the PSR and HPR on DoSi electrode and carbon felt electrode, respectively ($V_{DIR} = E_{S_2O_8^{2-}} - E_{H_2O_2} = 2.84\ V$). In each ModES cycle, the total voltage applied to this ModES system (i.e., $V_{ModES} = V_{cell,\ H_2O_2} + V_{cell,\ S_2O_8^{2-}}$) was 2.89 V on an average. This yielded a VE of around 98.3%,

Please cite this article in press as: Wang et al., Modular Electrochemical Synthesis Using a Redox Reservoir Paired with Independent Half-Reactions, Joule (2020), https://doi.org/10.1016/j.joule.2020.11.011

indicating minimal voltage and energy loss associated with the use of the solid-state RR in this membrane-free ModES system. In other words, the fast oxidation/reduction kinetics of the RR ensures that using the RR in a two-step electrochemical processes introduces very little potential/energy penalty in comparison with the direct electrolysis processes. In fact, the membrane needed for direct electrochemical cell usually imposes consideration of some factors, such as reaction selectivity, membrane stability, and a need for conditions that avoid membrane fouling.[17] Another interesting feature of ModES is that the cell voltages needed for each step ($V_{cell,\ H_2O_2}$ *and* $V_{cell,\ S_2O_8^{2-}}$) are both lower than the V_{DIR} due to the introduction of RR with a redox potential between $E_{S_2O_8^{2-}}$ and $E_{H_2O_2}$.

Furthermore, Figure 4D shows that this ModES process can consistently produce H_2O_2 and $Na_2S_2O_8$ for 100 continuous cycles (~36 h) without appreciable degradation in Faradaic efficiency (Figure 4D, top), VE (Figure 4D, bottom), and E_{RR} (Figure S19). Importantly, reasonably stable concentrations of H_2O_2 (~ 0.7 mM) and $Na_2S_2O_8$ (~ 0.4 mM) were consistently produced by the ModES system throughout the 100 operation cycles. The variations of FE and product concentration between cycle to cycle are due to the fluctuations of current and charge passing through the whole $Cell_{H_2O_2}$ and $Cell_{S_2O_8^{2-}}$ (Figure S18), caused by the variations of cell resistance, stirring speed, and O_2 bubbling rate (see Experimental Procedures). To further analyze the stability of the NaNiHCF-10 RR, we carried out PXRD characterization of the RR electrode after the 100-cycle operation (Figure S20), which revealed that the crystal structure of the RR electrode material showed no structural change during the ModES cycling processes. The excellent cycling stability of the RR electrode was also further confirmed by measuring the total capacity of the RR electrode randomly during this 100-cycle operation. The data showed a very low average capacity decay rate of 0.09%/cycle$_{\text{ModES}}$ (Figure S21 and, Section S3). Moreover, the RR electrode could also retain its capacity without self-reduction after being stored in the electrolyte for a long time (Figure S22) to ensure that HPR and PSR can be carried out at the desired time. Collectively, these results demonstrate that a well-designed heterogeneous RR can be continuously operated with high efficiency and good stability in ModES applications.

Advantages and Future Development of ModES

This ModES system generates two different high-value oxidants (H_2O_2 and $Na_2S_2O_8$) in practically useful concentrations in temporally separated steps by using a solid-state RR electrode. In contrast to conventional electrolysis, the production of H_2O_2 and $Na_2S_2O_8$ does not need to be coupled with sacrificial OER and HER processes that generate the O_2 and H_2 by-products, respectively, at the counter electrodes. These results set the stage for future design and development of new heterogeneous RR electrodes, and optimization of their size, form factors, and integration in stacked cells (Figure S23), to achieve higher and tunable product concentrations from the ModES system for different applications. Moreover, the co-production of H_2O_2 and $Na_2S_2O_8$ is accomplished without the use of expensive membranes to prevent undesired crossover of ions and products into different chambers.[17,47] Crossover of these highly reactive chemicals will result in reactions with each other and prevents the accumulation of high product concentrations, thus lowering the process efficiency. In addition, common polymer membranes are likely to be unstable long term in the presence of two strongly oxidizing reagents. The heterogeneous RR-based ModES system described here overcomes each of these challenges, since the cathodic and anodic electrolytes are never in direct contact with each other, and thus, the product crossover is minimized without using a membrane. Due to the modular and flexible nature of ModES

Please cite this article in press as: Wang et al., Modular Electrochemical Synthesis Using a Redox Reservoir Paired with Independent Half-Reactions, Joule (2020), https://doi.org/10.1016/j.joule.2020.11.011

strategy, both heterogeneous and homogeneous redox species can be used as the RRs. The homogeneous RR-enabled ModES system, where the anode and cathode chambers need to be separated by an ion-selective membrane to prevent mixing of produced chemicals, has some similarities to redox flow batteries (RFBs).[48] But, RFBs rely on two redox species with different redox potentials to store and release electrical energy, whereas homogeneous RR-enabled ModES systems only require one redox species to pair with different electrochemical reactions to produce chemicals. A point worth noting is that the membrane used in homogeneous RR-enabled ModES will introduce electrical resistance losses that can reduce the energy efficiency.

We anticipate that the ModES process demonstrated here may be readily adapted to other paired electrosynthesis to generate oxidative and reductive co-products without requiring optimization of a directly paired electrolysis process and without using expensive membranes. Moreover, previously unpaired cathodic and anodic half-reactions could be integrated in a ModES process to form a complete electrochemical reaction with minimal process design and optimization processes. To further demonstrate the generality of the ModES process for electrosynthesis of different chemicals, we combine another two previously unpaired reactions of HPR and production of active chlorine (AC) by using the same NaNiHCF-10 RR electrode. AC is a widely produced oxidant,[4,9] but its electrochemical production is usually coupled with HER as the cathodic reaction.[49,50] We first studied the AC production over the commercial dimensionally stable anode (DSA) in saturated NaCl electrolyte in a conventional cell (Figures S24 and S25). The LSV curve (Figure 5A, olive curve) shows that the anodic current increases after applying potential of 1.35 V_{SHE}. Furthermore, the Faradaic efficiencies of 91%–93% of AC production at the potential of 1.35–1.39 V_{SHE} (Figure 5A, red dots) were obtained by chronoamperometric measurement, followed by titration determination (Figure S25B; Section S4). Then, the ModES process was successfully conducted under the average cell voltage of ~0.85 V ($Cell_{H_2O_2}$) and ~0.56 V ($Cell_{AC}$) (see Experimental Procedures and Figures S26 and S27) to produce H_2O_2 and AC in the concentrations of around 0.56 and 0.5 mM, respectively, with the voltage efficiency (VE) close to 100% (Figures 5B and S27B). This example of producing another oxidant over a different anode and in a different electrolyte using the same RR demonstrates the flexibility of the ModES process.

The ModES approach could further serve as an integrated platform to support multiple electrochemical manufacturing processes for the production of both inorganic and organic chemicals.[5–7,9] As illustrated in Figure 5C, an idealized but relatively straightforward extension of the concept implemented here would incorporate suitably designed RR materials that allow cathodic and anodic reactions to be carried out on demand at different times, under different reaction conditions, and on different scales for multiple processes that are commensurate with the demands[7,14] in real time. Beyond our laboratory demonstration based on batch processing here, we may envision a prototype continuous flow ModES system (Figure 5C) that consists of a central electrochemical cell, in which, the stationary solid-state RR electrode and the cathode and anode are located, and multiple electrolyte (substrate) tanks for various pairing of oxidation/reduction processes. During the half-cycle for the oxidation reaction, the chosen anodic electrolyte (blue) is flowed into the central cell to be oxidized into the corresponding product together with the reduction of the RR. Next, during the reduction half-cycle, the cathodic electrolyte (red) is flowed into the central cell for reduction reaction together with the oxidation of the RR. With the help of automated flow control and electric switching systems, such ModES

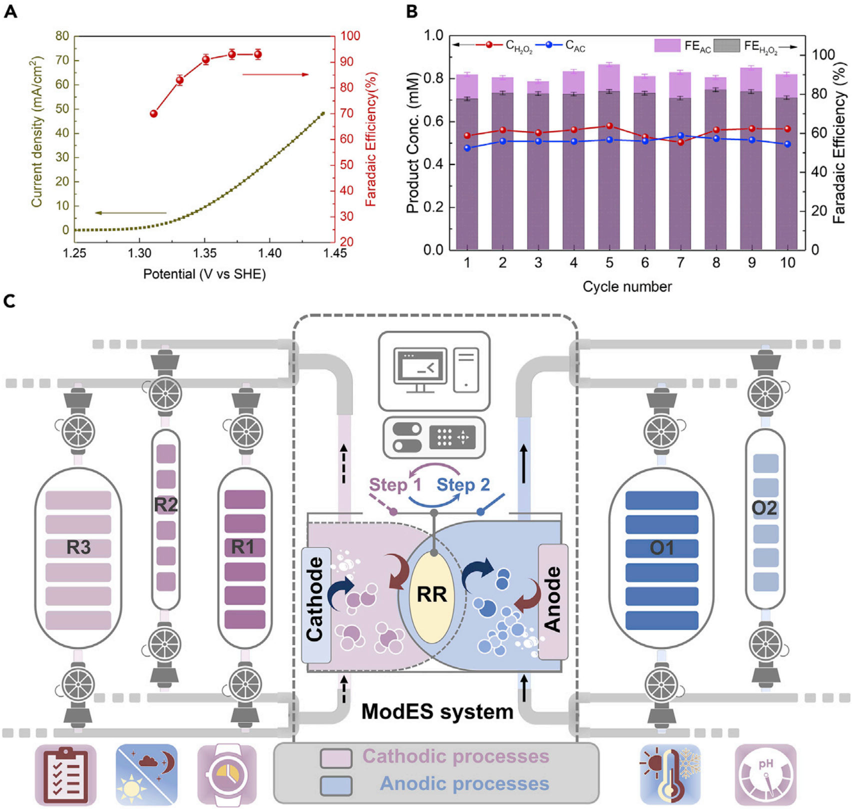

Figure 5. Expanding the Same ModES System to the Electrosynthesis of H_2O_2 and Active Chlorine (AC) and Schematic Illustration of an Envisioned ModES Flow Cell System for Integrated Modular Production of Multiple Chemicals

(A) LSV curve (without *iR* compensation) measured at a scan rate of 10 mV s^{-1} and the corresponding potential-dependent Faradaic efficiency of DSA electrode for producing AC in saturated NaCl electrolyte. The error bars shown are the confident intervals of the Faradaic efficiency at different potential.

(B) Modular production of H_2O_2 and AC, accumulating the concentrations of ~0.56 mM H_2O_2 (blue dots) and ~0.5 mM AC (red dots), along with the Faradaic efficiencies (bars) achieved in ten representative operation cycles using ModES. The error bars shown are the confident intervals of the product concentration and Faradaic efficiency.

(C) A central electrochemical cell, in which the stationary solid-state RR and the cathode and anode are located, can be combined with multiple electrolyte (substrate) from the cylinders on both sides for arbitrary pairing of various cathodic/anodic processes. During the electrosynthesis half-cycle of the oxidation products (such as $S_2O_8^{2-}$, ClO^-, O_2, etc.), the corresponding electrolyte (shown in blue) is flowed into the central cell to be in contact with the anode and the RR electrode; then, during the half-cycle of reduction products (such as H_2O_2, H_2, etc.), a different electrolyte (shown in red) is flowed into the central cell with the cathode and RR electrode. Prior to each half-reaction, the central electrochemical cell needs to be flushed with the incoming electrolyte. With the help of an automated control system and suitably designed RR electrode, this system can be operated in a cyclic continuous flow mode to enable the on-demand production of multiple chemicals in different scales, possibly at different times and reaction conditions.

system can be operated in a continuous and cyclic fashion to realize multiple electrochemical reactions to generate desired oxidation or reduction products in different scales at different times based on the demands.

Conclusions

This work presents a ModES approach to integrate two complementary redox reactions, electrochemical reduction of O_2 to H_2O_2 and oxidation of Na_2SO_4 to $Na_2S_2O_8$

Please cite this article in press as: Wang et al., Modular Electrochemical Synthesis Using a Redox Reservoir Paired with Independent Half-Reactions, Joule (2020), https://doi.org/10.1016/j.joule.2020.11.011

(or oxidation of Cl^- to active chlorine) by pairing the respective half-reactions with the oxidation and reduction of NaNiHCF material, which serves as a robust and electrochemically reversible heterogeneous redox reservoir. The ModES system can be continuously operated over 100 cycles to produce H_2O_2 and $Na_2S_2O_8$ with an excellent voltage efficiency. These strong oxidants are appealing targets for distributed manufacturing, bypassing the need to ship hazardous materials and allowing on-demand electrochemical production for biocide, disinfection, and environmental applications. The membrane-free ModES design offers many advantages over conventional paired electrolysis processes and would allow better utilization of renewable electricity generated by the intermittent and diffuse energy sources (such as solar or wind) for chemical manufacturing. To facilitate practical applications of such ModES processes, it is critical to further develop and improve new RR materials capable of reversible (most likely aqueous) redox reactions involving many electrons and a variety of ionic species to allow higher capacity, better cycling stability, and more chemical diversity. These novel ModES processes enabled by redox reservoirs, when combined with recent breakthroughs in electrocatalysis,[3,9] could further increase the efficiency and economic viability, and thus, accelerate the deployment of distributed electrochemical manufacturing processes.

EXPERIMENTAL PROCEDURES

Resource Availability

Lead Contact

Further information and requests for resources and materials should be directed to and will be fulfilled by the Lead Contact, Song Jin (jin@chem.wisc.edu).

Materials Availability

The materials generated in this study can be made available upon reasonable request.

Data and Code Availability

This study did not generate any computer code.

Material Synthesis and Structural Characterization

Sodium nickel hexacyanoferrate (NaNiHCF) samples were synthesized using an aqueous co-precipitation method.[35] Typically, 50 mL of $NiCl_2 \cdot 6H_2O$ (to make a solution concentration of 0.1 mol L^{-1}) and sodium citrate dihydrate solution (in different concentrations of 0.1, 0.5, 1.0, and 1.5 mol L^{-1}) mixed solution, and 50 mL 0.1 M $Na_4Fe(CN)_6$ solution were simultaneously added dropwise to 100 mL H_2O under vigorous stirring. The molar ratio between Ni^{2+} and citrate in the synthesis was 1: x (x = 1, 5, 10, 15), which is used to denote the products as NaNiHCF-x. The solution was then stirred for another 24 h, at room temperature for the NaNiHCF-1, 5 samples, and at 80°C for the NaNiHCF-10, 15 samples, to yield a light-green precipitate. This precipitate was centrifuged and then rinsed with deionized water multiple times and dried in a vacuum oven at 60°C overnight.

Powder X-ray diffraction (PXRD) patterns of different NaNiHCF-x samples were collected using a Bruker D8 Advance X-ray diffractometer equipped with Cu-Kα radiation. The size and morphology of the samples were characterized using a scanning electron microscope (SEM, Zeiss SUPRA 55VP) equipped with an energy dispersive X-ray spectroscopy (EDS) detector. Inductively coupled plasma-optical emission spectrometer (ICP-OES, Agilent 5110) was utilized to determine the compositions of Na, Ni, and Fe elements, and thermogravimetric analysis (TGA, TA Q500) was used to determine the water content in the various NaNiHCF-x samples.

X-ray photoelectron spectroscopy (XPS) was conducted on a Thermo Fisher Scientific *K*-Alpha spectrometer with a monochromatic Al-Kα X-ray source.

Fabrication and Electrochemical Tests of the RR Electrodes

To prepare the NaNiHCF electrodes, 70 wt % NaNiHCF-*x* powder, 20 wt % acetylene carbon black (Alfa Aesar) and 10 wt % polytetrafluoroethylene binder (Millipore Sigma) dispersed in de-ionized water were mixed and grounded using a mortar and pestle with a small amount of ethanol to form a paste, which was then kneaded and rolled into a film with a thickness of ~ 100–130 μm. The film was cut into different sizes, including 1 × 1 cm^2 and 2 × 2 cm^2, with square dies, and then dried in a vacuum oven at 60°C for 12 h to remove the residual solvent. The film was weighted and then pressed onto a titanium mesh current collector (150 mesh, with the thickness of ~ 230 μm) using a hydraulic press (Carver). The mass loading of NaNiHCF-*x* on the electrodes was around 8–10 mg/cm^2.

The electrochemical properties of NaNiHCF electrodes were characterized in 1.7 M Na_2SO_4 solution with a three-electrode configuration. A NaNiHCF electrode, a platinum mesh, and a saturated calomel electrode (SCE) were used as the working, counter, and reference electrodes, respectively. Cyclic voltammetry (CV) and galvanostatic cycling of the NaNiHCF electrodes were carried out using a Bio-Logic VMP-3 multichannel potentiostats. The galvanostatic cycling was performed at the rate of 100 mA g^{-1} for stability characterization and rates of 0.1 A g^{-1} to 10 A g^{-1} for kinetics characterization.

Electrochemical Measurements of the Electrocatalytic Electrodes

All electrocatalytic characterizations were performed using a Bio-Logic SP-200 potentiostat at room temperature. Hydrogen peroxide (H_2O_2) and sodium persulfate ($Na_2S_2O_8$) production reactions were first evaluated in H-cells with a Nafion 117 membrane (Sigma-Aldrich) and 1.7 M Na_2SO_4 electrolyte.

H_2O_2 Production and Detection

Carbon felt (2 × 3 cm^2, 3 mm thickness, GFD 3 EA, SIGRACELL®) was heated in air at 400°C for 24 h in a furnace, and then connected to a custom-made graphite clip current collector to serve as the working electrode. A graphite rod and a SCE were used as the counter and reference electrodes, respectively. Prior to the measurements, the electrolyte was purged with O_2 gas for 15 min. Then, the electrocatalytic activity of the carbon felt electrode was investigated in the electrolyte with vigorous stirring (1,000 r.p.m.) and continuous O_2 gas bubbling by CV and linear scan voltammetry (LSV) at 10 mV/s, and chronoamperometry (CA) at different potentials (0.1, 0.0, −0.1, −0.2, −0.3 V_{SHE}). All potentials measured against SCE were converted to the standard hydrogen electrode (SHE) scale using $E_{SHE} = E_{SCE} + 0.241$ V.

To determine the Faradaic efficiency (FE) for the H_2O_2 production reaction (HPR), the concentration of the H_2O_2 generated by CA was first roughly detected using standard H_2O_2 strips (Indigo Instruments, Figure S10B). The exact concentration was then further measured by the titration with ceric sulfate (Section S1).[39,42] The FE for HPR is calculated using the following equation:

$$FE\ (\%) = \frac{Q\ for\ H_2O_2\ production}{Q_{input}} \times 100 = \frac{[H_2O_2] \times V \times 2 \times 96485}{Q_{input}} \times 100 \qquad \text{(Equation 1)}$$

where V, $[H_2O_2]$ and Q_{input} are the volume of the electrolyte, concentration of produced H_2O_2 and the input charge during the electrolysis processes, respectively.

Please cite this article in press as: Wang et al., Modular Electrochemical Synthesis Using a Redox Reservoir Paired with Independent Half-Reactions, Joule (2020), https://doi.org/10.1016/j.joule.2020.11.011

Sodium Persulfate Production and Detection

BDD film with a thickness of 1 μm (resistivity <0.1 ohm-cm) on p type (100) silicon (resistivity of 0.01–0.02 ohm-cm) wafer (Lightning 25 DoSi wafer, Advanced Diamond Technologies Inc.) was used to fabricate the working electrode for $Na_2S_2O_8$ production reaction (PSR). The back side (Si side) of the DoSi wafer was first carefully cleaned using 24 wt % hydrofluoric acid to remove the silicon oxide, then an ohmic contact was made by attaching a piece of Cu foil fixed on a piece of glass slide onto the back side of the DoSi wafer with gallium-indium eutectic (Sigma-Aldrich). The whole ohmic contact area was sealed with epoxy resin (Loctite, EA9460). The detailed procedure is illustrated in Figure S14. The electrochemical measurements were performed with a three-electrode configuration, using a platinum-mesh electrode and a Hg/Hg_2SO_4 electrode (in saturated K_2SO_4, CH Instruments) as the counter and reference electrodes, respectively. CV and LSV were performed with a scan rate of 10 mV/s. The electrochemical impedance spectroscopy (EIS) analysis was carried out with a frequency range of 100 kHz to 100 mHz at open circuit potential to check the uncompensated resistance (R_u) of the electrochemical system, which revealed a low R_u of 2.3–3 Ω with the DoSi working electrode. CA was then carried out at potentials of 2.3, 2.5, 2.7, 2.8, 2.9, and 2.94 V_{SHE} for cumulative persulfate production. All potentials measured against Hg/Hg_2SO_4 ($E_{Hg/Hg2SO4}$) were converted to the SHE scale using $E_{SHE} = E_{Hg/Hg2SO4} + 0.64$ V.

The concentration of the sodium persulfate generated by CA was determined with a rapid spectrophotometric method based on iodometric titration (Section S2).[51] The reaction between persulfate and iodide (Equation 2) with the presence of sodium bicarbonate resulted in a yellow color with an absorbance at 352 nm.

$$S_2O_8^{2-} + 2I^- \rightarrow 2SO_4^{2-} + I_2 \qquad \text{(Equation 2)}$$

All sample solution analyses were conducted by taking 100 μL electrolytes containing $Na_2S_2O_8$ product after CA electrolysis processes. The FE for PSR is calculated using the following equation:

$$FE\ (\%) = \frac{Q\ for\ \left[S_2O_8^{2-}\right]\ production}{Q_{input}} \times 100 = \frac{\left[S_2O_8^{2-}\right] \times V \times 2 \times 96485}{Q_{input}} \times 100 \qquad \text{(Equation 3)}$$

Where, V, $[S_2O_8^{2-}]$, and Q_{input} are the volume of the electrolyte, concentration of produced $Na_2S_2O_8$, and the input charge during the CA electrolysis processes, respectively.

Active Chlorine Production and Detection

The active chlorine production reaction (ACR) was first evaluated in a H-cell with a glass filter separator (ACE glass Incorporated, USA) and saturated NaCl electrolyte. Commercial dimensionally stable anode (DSA, 1 × 3 cm^2), namely, iridium-ruthenium oxides covered Ti mesh ($IrRuO_x/Ti$), was used as the working electrode.[50,52] The electrochemical measurements were performed with a three-electrode configuration, using a platinum-mesh electrode and a SCE electrode as the counter and reference electrodes, respectively. CV and LSV was performed with a scan rate of 10 mV/s (Figure S25A), and CA was carried out at different potentials (1.311, 1.331, 1.351, 1.371, and 1.391 V_{SHE}) with stirring (1,000 r.p.m.) (Figure S25B). All potentials measured against SCE were converted to SHE using $E_{SHE} = E_{SCE} + 0.241$ V. The concentration of the produced active chlorine was measured by the iodometric method (see Section S4).[53] The FE for ACR were then calculated based on the concentration of active chlorine and input charge.

Please cite this article in press as: Wang et al., Modular Electrochemical Synthesis Using a Redox Reservoir Paired with Independent Half-Reactions, Joule (2020), https://doi.org/10.1016/j.joule.2020.11.011

Demonstration of RR-Enabled ModES Process

To demonstrate the production of H_2O_2 and $Na_2S_2O_8$ in a ModES system, two electrolysis cells, H_2O_2 cell ($Cell_{H_2O_2}$) and $Na_2S_2O_8$ cell ($Cell_{S_2O_8^{2-}}$), each containing 35 mL of 1.7 M Na_2SO_4 electrolyte were used. A NaNiHCF-10 RR electrode (2 × 2 cm^2, ~36.5 mg active material loading) was used as the counter electrode in both cells. In $Cell_{H_2O_2}$, a heat-treated carbon felt electrode (2 × 3 cm^2), and an SCE were utilized as the working and reference electrode, respectively. O_2 gas was continuously bubbled in the solution to ensure O_2 saturation. In $Cell_{S_2O_8^{2-}}$, a DoSi electrode (2 × 2 cm^2) and a Hg/Hg_2SO_4 electrode were used as the working and reference electrode, respectively. As illustrated in Figure S17, in $Cell_{H_2O_2}$, the RR electrode was oxidized to RR^{ox} and released the stored electrons, and O_2 was reduced on the carbon felt electrode at −0.1 V_{SHE} to generate H_2O_2. After being oxidized to the desired SOR, the RR^{ox} electrode was taken out of $Cell_{H_2O_2}$, washed with Na_2SO_4 solution, and then moved to $Cell_{S_2O_8^{2-}}$. In $Cell_{S_2O_8^{2-}}$, the RR^{ox} electrode was reduced (to form RR^{red}) to "store" electrons and $SO_4{}^{2-}$ was oxidized on the DoSi electrode at 2.74 V_{SHE} to generate $S_2O_8{}^{2-}$. Additionally, the potential of the RR electrode was monitored, which was used to calculate the total cell voltage (V_{cell}), i.e., the potential difference between the RR electrode and carbon felt or DoSi electrode. During these ModES cycles, the capacity change of the RR electrode was controlled by the potential to make sure the RR electrode was operated within the desired SOR range. The concentrations of the produced H_2O_2 and $Na_2S_2O_8$ were measured following the procedures described above as a function of capacity utilization rate within a ModES cycle. Based on the product concentrations, the Faradaic efficiencies were calculated according to the following equation:

$$FE(\%)_{H_2O_2} = \frac{Q\ for\ H_2O_2\ production}{Q_{passing,\ RR}} \times 100 = \frac{[H_2O_2] \times V \times 2 \times 96485}{Q_{passing,\ RR}} \times 100 \quad \text{(Equation 4)}$$

$$FE(\%)_{S_2O_8^{2-}} = \frac{Q\ for\ \left[S_2O_8^{2-}\right]\ production}{Q_{passing,\ RR}} \times 100 = \frac{\left[S_2O_8^{2-}\right] \times V \times 2 \times 96485}{Q_{passing,\ RR}} \times 100 \quad \text{(Equation 5)}$$

where, the $Q_{passing,\ RR}$ is the charge passing through RR electrode in $Cell_{H_2O_2}$ and $Cell_{S_2O_8^{2-}}$.

For the long-term ModES system cycling test, another RR electrode (2 × 2 cm^2, ~36.5 mg active material loading) was used, which was pre-oxidized at 10 mA (~274 mA/g_{active}) to 25% SOR (i.e., 0.7 V_{SHE}) in the same electrolyte (1.7 M Na_2SO_4). In one ModES cycle, the RR electrode was first oxidized from 25% to 75% SOR (i.e., 0.78 V_{SHE}, the utilized capacity of ~ 4.6 C) in $Cell_{H_2O_2}$ to produce H_2O_2, followed by being reduced from 75% to 25% SOR in the $Cell_{S_2O_8^{2-}}$ to produce $Na_2S_2O_8$. This ModES system was continuously operated for 100 cycles using the same RR electrode (Figures 4D and S19).

To demonstrate the production of H_2O_2 and AC using the ModES system, two electrolysis cells, H_2O_2 cell ($Cell_{H_2O_2}$) and AC cell ($Cell_{AC}$), each containing ~35 mL 1.7 M Na_2SO_4 and saturated NaCl, respectively, were used. The same NaNiHCF-10 RR electrode was used as the counter electrode in both cells (Figure S26). In $Cell_{H_2O_2}$, O_2 was reduced on the carbon felt electrode at −0.1 V_{SHE} to generate H_2O_2 and the RR electrode was oxidized to RR^{ox}. After being oxidized to the desired SOR, the RR^{ox} electrode was washed with NaCl solution and then moved to $Cell_{AC}$. In $Cell_{AC}$, a DSA electrode (1 × 3 cm^2) and SCE were used as the working and reference electrode, respectively. And the AC was produced on the DSA electrode at the potential of 1.331 V_{SHE}. Around 50% SOR (~ 4.3 C) of the NaNiHCF-10 RR electrode was utilized during the separate production of H_2O_2 and AC for multiple ModES cycles. Based on the product concentrations in each cycle, the Faradaic efficiencies were also calculated accordingly.

SUPPLEMENTAL INFORMATION

Supplemental Information can be found online at https://doi.org/10.1016/j.joule.2020.11.011.

ACKNOWLEDGMENTS

This work is supported by the University of Wisconsin-Madison UW2020 grant. F.W. also acknowledges the support from China Scholarship Council (CSC), National Natural Science Foundation of China (no. 21805057), and CAS Key Laboratory of Nanosystem and Hierarchical Fabrication. T.G. acknowledges the support from the International Postdoctoral Exchange Fellowship Program of China. S.S.S. is also supported by the Center for Molecular Electrocatalysis, an Energy Frontier Research Center funded by the U.S. Department of Energy, Office of Science, Office of Basic Energy Sciences. The authors thank Prof. T.W. Root for reading the manuscript and providing useful suggestions for improving Figure 5C.

AUTHOR CONTRIBUTIONS

F.W., W.L., and S.J. conceived the idea and designed the experiments. F.W. and W.L. synthesized the redox reservoir materials, F.W. performed the electrochemical tests and analyzed the data. R.W. conducted the active chlorine production and analyzed the data. T.G. assisted in the experiments on production of chemicals in ModES system, H.S. assisted in hydrogen peroxide production and electrode characterization. H.F. assisted in the electrode fabrication for persulfate production. S.J. and S.S.S. supervised the project. F.W., W.L., S.S.S., and S.J. wrote the manuscript. All authors contributed to the overall scientific interpretation and edited the manuscript.

DECLARATION OF INTERESTS

The authors declare no competing financial interests.

Received: September 17, 2020
Revised: October 8, 2020
Accepted: November 12, 2020
Published: December 11, 2020

REFERENCES

1. Chu, S., Cui, Y., and Liu, N. (2016). The path towards sustainable energy. Nat. Mater. *16*, 16–22.
2. Wiebe, A., Gieshoff, T., Möhle, S., Rodrigo, E., Zirbes, M., and Waldvogel, S.R. (2018). Electrifying organic synthesis. Angew. Chem. Int. Ed. Engl. *57*, 5594–5619.
3. Seh, Z.W., Kibsgaard, J., Dickens, C.F., Chorkendorff, I., Nørskov, J.K., and Jaramillo, T.F. (2017). Combining theory and experiment in electrocatalysis: insights into materials design. Science *355*, eaad4998.
4. Botte, G.G. (2014). Electrochemical manufacturing in the chemical industry. Electrochem. Soc. Interface *23*, 49–55.
5. Cardoso, D.S.P., Šljukić, B., Santos, D.M.F., and Sequeira, C.A.C. (2017). Organic electrosynthesis: from laboratorial practice to industrial applications. Org. Process Res. Dev. *21*, 1213–1226.
6. Couper, A.M., Pletcher, D., and Walsh, F.C. (1990). Electrode materials for electrosynthesis. Chem. Rev. *90*, 837–865.
7. Palmer, C., Saadi, F., and McFarland, E.W. (2018). Technoeconomics of commodity chemical production using sunlight. ACS Sustainable Chem. Eng. *6*, 7003–7009.
8. Montoya, J.H., Seitz, L.C., Chakthranont, P., Vojvodic, A., Jaramillo, T.F., and Nørskov, J.K. (2016). Materials for solar fuels and chemicals. Nat. Mater. *16*, 70–81.
9. Martín, A.J., and Pérez-Ramírez, J. (2019). Heading to distributed electrocatalytic conversion of small abundant molecules into fuels, chemicals, and fertilizers. Joule *3*, 2602–2621.
10. Stamenkovic, V.R., Strmcnik, D., Lopes, P.P., and Markovic, N.M. (2016). Energy and fuels

Please cite this article in press as: Wang et al., Modular Electrochemical Synthesis Using a Redox Reservoir Paired with Independent Half-Reactions, Joule (2020), https://doi.org/10.1016/j.joule.2020.11.011

from electrochemical interfaces. Nat. Mater. *16*, 57–69.

11. Aust, N., and Kirste, A. (2014). Paired Electrosynthesis. In: Kreysa G., Ota K., Savinell R.F. (eds) Encyclopedia of Applied Electrochemistry (Springer), pp. 1505–1510.
12. Martínez, N.P., Isaacs, M., and Nanda, K.K. (2020). Paired electrolysis for simultaneous generation of synthetic fuels and chemicals. New J. Chem. *44*, 5617–5637.
13. Putter, H., and Hannebaum, H. (2000). Preparation of phthalides. U.S Patent *6063256*.
14. Verma, S., Lu, S., and Kenis, P.J.A. (2019). Co-electrolysis of CO_2 and glycerol as a pathway to carbon chemicals with improved technoeconomics due to low electricity consumption. Nat. Energy *4*, 466–474.
15. Rausch, B., Symes, M.D., Chisholm, G., and Cronin, L. (2014). Decoupled catalytic hydrogen evolution from a molecular metal oxide redox mediator in water splitting. Science *345*, 1326–1330.
16. Wallace, A.G., and Symes, M.D. (2018). Decoupling strategies in electrochemical water splitting and beyond. Joule *2*, 1390–1395.
17. Paidar, M., Fateev, V., and Bouzek, K. (2016). Membrane electrolysis—history, current status and perspective. Electrochim. Acta *209*, 737–756.
18. Dotan, H., Landman, A., Sheehan, S.W., Malviya, K.D., Shter, G.E., Grave, D.A., Arzi, Z., Yehudai, N., Halabi, M., Gal, N., et al. (2019). Decoupled hydrogen and oxygen evolution by a two-step electrochemical–chemical cycle for efficient overall water splitting. Nat. Energy *4*, 786–795.
19. Chen, L., Dong, X., Wang, Y., and Xia, Y. (2016). Separating hydrogen and oxygen evolution in alkaline water electrolysis using nickel hydroxide. Nat. Commun. *7*, 11741.
20. Chen, J.J., Symes, M.D., and Cronin, L. (2018). Highly reduced and protonated aqueous solutions of $[P_2W_{18}O_{62}]_{6-}$ for on-demand hydrogen generation and energy storage. Nat. Chem. *10*, 1042–1047.
21. Landman, A., Dotan, H., Shter, G.E., Wullenkord, M., Houaijia, A., Maljusch, A., Grader, G.S., and Rothschild, A. (2017). Photoelectrochemical water splitting in separate oxygen and hydrogen cells. Nat. Mater. *16*, 646–651.
22. Symes, M.D., and Cronin, L. (2013). Decoupling hydrogen and oxygen evolution during electrolytic water splitting using an electron-coupled-proton buffer. Nat. Chem. *5*, 403–409.
23. Landman, A., Halabi, R., Dias, P., Dotan, H., Mehlmann, A., Shter, G.E., Halabi, M., Naseraldeen, O., Mendes, A., Grader, G.S., et al. (2020). Decoupled photoelectrochemical water splitting system for centralized hydrogen production. Joule *4*, 448–471.
24. Campos-Martin, J.M., Blanco-Brieva, G., and Fierro, J.L.G. (2006). Hydrogen peroxide synthesis: an outlook beyond the anthraquinone process. Angew. Chem. Int. Ed. Engl. *45*, 6962–6984.
25. Chadwick, S.S. (2007). Ullmann's Encyclopedia of Industrial Chemistry (Wiley-VCH Verlag).
26. Perry, S.C., Pangotra, D., Vieira, L., Csepei, L., Sieber, V., Wang, L., Ponce de León, C., and Walsh, F.C. (2019). Electrochemical synthesis of hydrogen peroxide from water and oxygen. Nat. Rev. Chem. *3*, 442–458.
27. IMARC (2020). Hydrogen peroxide market: global industry trends, share, size, growth, opportunity and forecast 2020–2025. https://www.imarcgroup.com/hydrogen-peroxide-technical-material-market-report.
28. MarketsandMarkets Research Private Ltd (2020). Persulfates Market by Type (Ammonium, Sodium, & Potassium),End-Use Industry (Polymer, Electronics and Cosmetic & Personal Care), Application (Polymer Initiator, Oxidation, Bleaching and Sizing Agent) and Region - Global Forecast to 2025. https://www.marketsandmarkets.com/Market-Reports/persulfates-market-59168451.html.
29. Anson, C.W., and Stahl, S.S. (2019). Processes for electrochemical production of electrolyte-free hydrogen peroxide. Joule *3*, 2889–2891.
30. Yang, S., Verdaguer-Casadevall, A., Arnarson, L., Silvioli, L., Čolić, V., Frydendal, R., Rossmeisl, J., Chorkendorff, I., and Stephens, I.E.L. (2018). Toward the decentralized electrochemical production of H_2O_2: A focus on the catalysis. ACS Catal. *8*, 4064–4081.
31. Zhu, J., Hii, K.K., and Hellgardt, K. (2016). Toward a green generation of oxidant on demand: practical electrosynthesis of ammonium persulfate. ACS Sustainable Chem. Eng. *4*, 2027–2036.
32. Bin, D., Wang, F., Tamirat, A.G., Suo, L., Wang, Y., Wang, C., and Xia, Y. (2018). Progress in aqueous rechargeable sodium-ion batteries. Adv. Energy Mater. *8*, 1703008.
33. Wu, X., Hong, J.J., Shin, W., Ma, L., Liu, T., Bi, X., Yuan, Y., Qi, Y., Surta, T.W., Huang, W., et al. (2019). Diffusion-free Grotthuss topochemistry for high-rate and long-life proton batteries. Nat. Energy *4*, 123–130.
34. Wessells, C.D., Huggins, R.A., and Cui, Y. (2011). Copper hexacyanoferrate battery electrodes with long cycle life and high power. Nat. Commun. *2*, 550.
35. Wu, X., Sun, M., Guo, S., Qian, J., Liu, Y., Cao, Y., Ai, X., and Yang, H. (2015). Vacancy-free Prussian Blue nanocrystals with high capacity and superior cyclability for aqueous sodium-ion batteries. ChemNanoMat *1*, 188–193.
36. Wang, L., Lu, Y., Liu, J., Xu, M., Cheng, J., Zhang, D., and Goodenough, J.B. (2013). A superior low-cost cathode for a Na-Ion battery. Angew. Chem. Int. Ed. Engl. *52*, 1964–1967.
37. Ji, Z., Han, B., Liang, H., Zhou, C., Gao, Q., Xia, K., and Wu, J. (2016). On the mechanism of the improved operation voltage of rhombohedral nickel hexacyanoferrate as cathodes for sodium-ion batteries. ACS Appl. Mater. Inter. *8*, 33619–33625.
38. Qian, J., Wu, C., Cao, Y., Ma, Z., Huang, Y., Ai, X., and Yang, H. (2018). Prussian Blue cathode materials for sodium-ion batteries and other ion batteries. Adv. Energy Mater. *8*, 1702619.
39. Lu, Z., Chen, G., Siahrostami, S., Chen, Z., Liu, K., Xie, J., Liao, L., Wu, T., Lin, D., Liu, Y., et al. (2018). High-efficiency oxygen reduction to hydrogen peroxide catalysed by oxidized carbon materials. Nat. Catal. *1*, 156–162.
40. Li, W., Zheng, J., Hu, B., Fu, H.C., Hu, M., Veyssal, A., Zhao, Y., He, J.H., Liu, T.L., Ho-Baillie, A., et al. (2020). High-performance solar flow battery powered by a perovskite/silicon tandem solar cell. Nat. Mater. *19*, 1326–1331.
41. Kim, H.W., Ross, M.B., Kornienko, N., Zhang, L., Guo, J., Yang, P., and McCloskey, B.D. (2018). Efficient hydrogen peroxide generation using reduced graphene oxide-based oxygen reduction electrocatalysts. Nat. Catal. *1*, 282–290.
42. Sheng, H., Hermes, E.D., Yang, X., Ying, D., Janes, A.N., Li, W., Schmidt, J.R., and Jin, S. (2019). Electrocatalytic production of H_2O_2 by selective oxygen reduction using earth-abundant cobalt pyrite (CoS_2). ACS Catal. *9*, 8433–8442.
43. Pletcher, D., and Walsh, F.C. (2012). Industrial Electrochemistry (Springer Science & Business Media).
44. Radimer, K. J. and Mccarthy, M. J. (1979). Electrolytic production of sodium persulfate. U.S Patent 4,144,144.
45. Davis, J., Baygents, J.C., and Farrell, J. (2014). Understanding persulfate production at boron doped diamond film anodes. Electrochim. Acta *150*, 68–74.
46. Yang, N., Yu, S., Macpherson, J.V., Einaga, Y., Zhao, H., Zhao, G., Swain, G.M., and Jiang, X. (2019). Conductive diamond: synthesis, properties, and electrochemical applications. Chem. Soc. Rev. *48*, 157–204.
47. Esposito, D.V. (2017). Membraneless electrolyzers for low-cost hydrogen production in a renewable energy future. Joule *1*, 651–658.
48. Luo, J., Hu, B., Hu, M., Zhao, Y., and Liu, T.L. (2019). Status and prospects of organic redox flow batteries toward sustainable energy storage. ACS Energy Lett. *4*, 2220–2240.
49. Thomas, F., O'Brien, T.V.B., and Hine, F. (2015). Handbook of Chlor-Alkali Technology (Springer Science & Business Media).
50. Matousek, R. (2014). Hypochlorite Synthesis Cells and Technology, Sea Water. In Encyclopedia of Applied Electrochemistry (Springer New York), pp. 1066–1070.
51. Liang, C., Huang, C.F., Mohanty, N., and Kurakalva, R.M. (2008). A rapid spectrophotometric determination of persulfate anion in ISCO. Chemosphere *73*, 1540–1543.
52. Zaviska, F., Drogui, P., Blais, J.-F., and Mercier, G. (2009). In situ active chlorine generation for the treatment of dye-containing effluents. J. Appl. Electrochem. *39*, 2397–2408.
53. R.B. Baird, A.D. Eaton, and E.W. Rice, eds. (2017). Standard methods for the examination of water and wastewater, 23rd Edition.